Journal of the European Ceramic Society **14** (1994) 539–548

Uniaxial Tensile and Creep Behaviour of an Alumina Fibre-Reinforced Ceramic Matrix Composite: II. Modelling of Tertiary Creep

F. Lamouroux, J. L. Vallés & M. Steen

Institute for Advanced Materials, Joint Research Centre, European Commission, PO Box 2, 1755 ZG Petten, The Netherlands

(Received 18 April 1994; accepted 17 May 1994)

Abstract

The tertiary creep of an alumina fibre-reinforced silicon carbide composite is modelled on the basis of the damage mechanisms activated during tensile creep tests carried out under vacuum at 1100°C. Progressive fibre–matrix debonding induced by the difference between the radial creep strain of the fibres and that of the matrix mantle is used to explain the axial creep behaviour. Fibre failure and the subsequent stress redistribution are also taken into account. The modelling approach successfully describes: (i) the time evolution of the creep rate, (ii) the decrease of the elastic modulus, (iii) the failure mode after tertiary creep and (iv) the stress dependence of the creep rate in the secondary stage and of the time to rupture of the composite. It is shown that a conventional creep stress exponent cannot be determined in this and similar composite materials because of the stress dependence of the damage accumulated in the composite before the secondary stage is reached.

Es wird ein Modell für das tertiäre Kriechen eines aluminiumoxidfaserverstärkten Siliziumcarbidverbundwerkstoffs entworfen. Die Grundlage hierfür bilden die Schädigungsmechanismen während einachsiger Kriechversuche unter Vakuum bei 1100°C. Das Kriechverhalten wird durch das fortschreitende Ablösen von Fasern von der Matrix erklärt, welches durch den Unterschied in der radialen Kriechdehnung der Fasern gegenüber der Matrix verursacht wird. Das Versagen der Fasern und die dadurch bewirkte Spannungsumverteilung werden ebenfalls in Rechnung gestellt. Diese mathematische Behandlung ist in der Lage, die folgenden Punkte erfolgreich zu beschreiben: (i) die Zeitabhängigkeit der Kriechrate, (ii) die zeitliche Abnahme des E-Moduls (iii) die Versagensmechanismen am Ende des tertiären Kriechens und (iv) die Spannungsabhängigkeit der Kriechrate im sekundären Bereich und der Zeit bis zum Versagen des Verbundwerkstoffs. Es wird gezeigt, daß für dieses Material und ähnliche Verbundwerkstoffe kein klassischer Spannungsexponent bestimmt werden kann. Der Grund hierfür liegt in der Tatsache, daß die Schädigung vor dem Erreichen des sekundären Bereichs spannungsabhängig ist.

Le fluage tertiaire d'un composite, constitué de fibres d'alumine et d'une matrice en carbure de silicium, est modélisé sur la base des mécanismes d'endommagement activés durant les tests de fluage uniaxiaux réalisés sous vide à 1100°C. Le mécanisme de décohésion fibre-matrice, induit par la différence de déformation radiale pendant le fluage des fibres dans les gaines de matrice, est utilisé pour expliquer le comportement en fluage uniaxial. La rupture des fibres et la redistribution des contraintes sont prises en considération. Ce modèle décrit avec succès: (i) l'évolution avec le temps de la vitesse de déformation, (ii) la décroissance du module d'elasticité, (iii) le mode de rupture à l'issue du stade tertiaire et (iv) la dépendance avec la contrainte de la vitesse de fluage au stade stationnaire et du temps de rupture du composite. Il est montré qu'un exposant de contrainte ne peut être déterminé de façon classique pour ce type de matériau, à cause de la dépendance avec le niveau des contraintes du taux d'endommagement du composite au stade secondaire.

1 Introduction

Ceramic fibre-reinforced ceramic matrix composites (CMCs) are envisaged as the most promising materials for structural applications at elevated temperatures. Besides being highly refractory and

Journal of the European Ceramic Society 0955-2219/94/$7.00

resistant to chemical attack, these materials do not present the low toughness of ceramics. Instead, they exhibit high damage tolerance and a good impact resistance both coupled to an extended non-linear regime under tensile loading. This mechanical behaviour is related to the development of damage. The damage mechanisms activated in a 2D Al_2O_3(f)/SiC composite during uniaxial tensile and creep tests have been studied on the basis of the elastic response and morphological analyses both after composite failure and *in situ* at room temperature.[1] For these composites having a creep mismatch ratio higher than one, i.e. when the creep rate of the fibres exceeds that of the matrix material, matrix microcracking is expected to be the dominant damage mode.[2] From the experimental study, it appears that, in addition to matrix microcracking, interfacial debonding and fibre rupture also play a role in the evolution of the composite strain rate during creep at 1100°C. The creep behaviour of alumina fibre-reinforced silicon carbide matrix composites has recently been the object of several experimental and modelling studies, which focused mainly on the description of the primary and secondary stages.[3–5] In the primary stage, a stress redistribution between matrix and longitudinal fibres takes place, which is influenced by matrix microcracking. At the end of this transient stage, an extended tertiary stage develops until composite failure occurs. The secondary stage is thus reduced to an inflection point in the creep curve. The first part of the tertiary stage has been associated to a progressive fibre–matrix debonding induced by a difference in the radial strains of both constituents.[1] This damage mechanism can account for the decrease of the longitudinal elastic modulus during tertiary creep, for the presence of large cracks in the matrix (of the order of 100 μm) and for the large amount of fibre pull-out observed on the fracture surface after creep failure.

In the present work, a modelling approach is developed in order to achieve a better understanding of the creep behaviour of Al_2O_3(f)/SiC composites during the tertiary stage. This allows a characterisation of the differences observed in the creep behaviour at low and high stresses, in particular in the evolution of the strain rate and in the creep failure mode.

2 Modelling Approach

In the experimental study described in the companion paper[1] it is shown that the increase of the creep strain rate in the Al_2O_3(f)/SiC composite is associated to a decrease of the longitudinal elastic modulus (Fig. 1). Such a change in the elastic

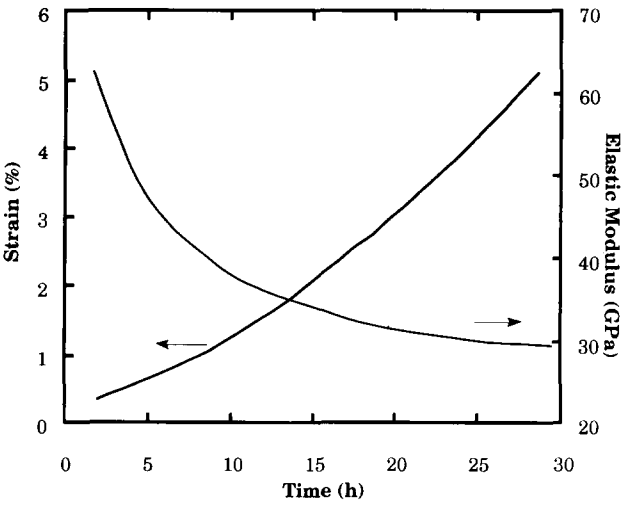

Fig. 1. Evolution of the axial strain and the longitudinal elastic modulus during tertiary creep of a 2D alumina fibre-reinforced SiC composite at 1100°C and under 100 MPa.

response cannot be caused by a multiplication of the cracks in the matrix, because the average crack spacing after creep failure is found to be similar to that observed right after loading. Besides, the final value reached by the elastic modulus corresponds to the theoretical stiffness of a totally debonded composite. As a consequence, a progressive fibre–matrix decohesion process is expected to occur during the earlier part of the tertiary creep stage. On the basis of this interfacial debonding and the ulterior process of fibre failure, modelling can provide an understanding about (i) the increase in the creep rate, (ii) the evolution of the elastic modulus, (iii) the creep rupture mode and (iv) the stress dependence of the creep behaviour.

In order to model the composite, a microcomposite consisting of an alumina fibre inside a silicon carbide mantle is first considered. The fibre volume fraction in the microcomposite corresponds to that in the composite in the axial direction and it is taken to be half of V_f, the total fibre volume fraction of the composite. The microcomposite matrix exhibits microcracks which are perpendicular to the fibre axis. They result from the mismatch between the coefficients of thermal expansion of fibre and matrix and they appear during the cooling step at the end of the manufacturing process. Therefore, the microcomposite model can be conceived as a series of blocks of different lengths, each composed of two distinct regions (see Fig. 2): an inner region where the fibre is perfectly bonded to the matrix, and an outer one, ending at a matrix crack, where it is completely debonded. In this approach, no friction is considered to occur at the interface during relative displacements between fibre and matrix. A more realistic interface[5] would take into account an intermediate region between the two, where friction plays a role. Certainly,

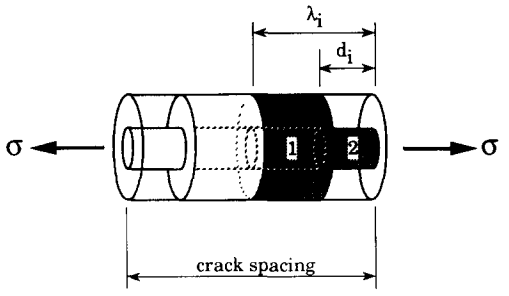

Fig. 2. Representation of a block in the microcomposite model. It is delimited by two matrix cracks and composed of two distinct regions: (1) the perfectly bonded region and (2) the totally debonded region.

during unloading–reloading excursions from the creep stress hysteresis loops were observed,[1] which are known to be related to interfacial friction.[6] Since the loop area remained unchanged during most of the creep test, the interfacial friction may be assimilated to a constant force offering resistance to the debonding process. In the present model, friction phenomena will be implicitly incorporated through the debonding rate parameter β, which is defined as the rate at which the fibre mechanically debonds from the matrix.

At the end of the tertiary stage the composite has undergone total fibre–matrix debonding, and it can better be modelled by a bundle of equivalent loose fibres. The application of a statistical approach then provides information on the time to rupture of the composite and on the possible catastrophic nature of the fibre failure process.

2.1 Creep rate during tertiary creep

The creep behaviour of the Sumitomo alumina fibre presents a primary and a secondary stage,[7] the latter being characterised by a constant creep rate $\dot{\varepsilon}_f$. Since the fibre creep rate exceeds that of the silicon carbide matrix, the axial creep expansion will induce a radial shrinkage of the fibre with respect to the matrix, and consequently it will promote interfacial debonding.[1] The fibre creep rate being constant during its secondary regime, it may be assumed that debonding progresses at a constant rate, called β. In the perfectly bonded region at the core of a microcomposite elementary block, the strain rate is limited by the silicon carbide matrix, the constituent with the lower creep rate. In contrast, in the debonded outer block region, as well as in the region of exposed fibre corresponding to a matrix crack, the fibre creep rate controls the deformation process. Because of the large difference in the creep rates of fibre and matrix, it may be assumed that the strain rate of a block composed of the two regions is given, in first approximation, by the strain rate of the debonded part. Thus,

$$\dot{\varepsilon}_i(t) = \dot{\varepsilon}_f X_i(t) \tag{1}$$

where $\dot{\varepsilon}_i$ is the strain rate of block i and X_i is its debonded fraction, defined as the ratio of the length of the debonded region ($2d_i$) to the total block length ($2\lambda_i$), i.e. $X_i = d_i/\lambda_i$. This equation applies as long as the composite presents a non-negligible debonded part.

Since a constant debonding rate is assumed, the time dependence of half the size of the debonded region in block i is given by

$$d_i(t) = d_i(0) + \beta t \tag{2}$$

where the time origin $t = 0$ corresponds to the start of the tertiary stage, and the debonded fraction evolves as

$$X_i(t) = X_i(0) + \frac{\beta}{\lambda_i} t \tag{3}$$

These expressions are valid until complete debonding of block i (or $X_i = 1$) is reached at a time:

$$t_i = \frac{\lambda_i}{\beta}(1 - X_i(0)) \tag{4}$$

Integration of eqn (1) with respect to time, and substituting for $X_i(t)$ according to eqn (3), provide the time evolution of the strain for block i of the microcomposite

$$t \le t_i \quad \varepsilon_i(t) = \varepsilon_i(0) + \dot{\varepsilon}_f\left(X_i(0)t + \frac{\beta}{2\lambda_i} t^2\right) \tag{5a}$$

$$t > t_i \quad \varepsilon_i(t) = \varepsilon_i(t_i) + \dot{\varepsilon}_f(t - t_i) \tag{5b}$$

where $\varepsilon_i(0)$ is the initial strain of block i, which is that accumulated until the onset of tertiary creep, and $X_i(t > t_i) = 1$ after total debonding.

The creep strain of the microcomposite can be calculated as the sum of the creep elongation of the blocks, divided by its total initial length. The expression obtained is:

$$\begin{aligned}\varepsilon(t) = \frac{\left(\sum_{i=1}^{n} \varepsilon_i(t)\lambda_i\right)}{\sum_{i=1}^{n} \lambda_i} &= \varepsilon(0) + \frac{\dot{\varepsilon}_f}{\sum_{i=1}^{n} \lambda_i} \\ &\times \left\{\sum_{i=1}^{n} \lambda_i \left[\left(X_i(0)t + \frac{\beta}{2\lambda_i} t^2\right)(1 - H(t; t_i))\right]\right\} \\ &+ \frac{\dot{\varepsilon}_f}{\sum_{i=1}^{n} \lambda_i} \left\{\sum_{i=1}^{n} \lambda_i \left[\left((t - t_i)\right.\right.\right. \\ &\left.\left.\left. + \left(X_i(0)t_i + \frac{\beta}{2\lambda_i} t_i^2\right)\right) H(t; t_i)\right]\right\}\end{aligned} \tag{6}$$

where $H(t; t_i)$ is Heaviside's step function, defined by $H(t; t_i) = 0$ for $t < t_i$ and $H(t; t_i) = 1$ for $t \ge t_i$.

When none of the microcomposite blocks has yet reached total debonding, i.e. in the case of

$t < \min(t_i)$, the total strain adopts the simpler expression

$$\varepsilon(t) = \varepsilon(0) + \dot{\varepsilon}_f \left(X(0)t + \frac{\beta}{2\bar{\lambda}} t^2 \right) \tag{7a}$$

where the microcomposite fraction of debonded fibre is

$$X(t) = \frac{\left(\sum_{i=1}^{n} \lambda_i \cdot X_i(t) \right)}{\sum_{i=1}^{n} \lambda_i} \tag{7b}$$

and $\bar{\lambda}$ is half the average length of a block. The latter can be taken as half the average matrix crack spacing $\bar{p}$, which can be determined from the crack spacing distribution obtained by means of optical analysis.[1] From eqn (7a), the strain rate of the microcomposite for $t < \min(t_i)$ is then

$$\dot{\varepsilon}(t) = \dot{\varepsilon}_f \left(X(0) + \frac{2\beta}{\bar{p}} t \right) \tag{8}$$

which is a linear function of time. When the first block becomes totally debonded, the derivative of the strain rate of the microcomposite starts to decrease. The strain rate becomes constant when all blocks of the microcomposite are totally debonded. The hypothesis that the creep of the microcomposite before complete debonding of any elementary block will faithfully represent that of the composite is based on the fact that, since the strain range attained during creep (2–8%) is quite large, the effect of the 2D woven texture on the mechanical behaviour can be neglected in first approximation.

From a single test, say that performed at 100 MPa, it is possible to determine the debonding rate β, which is only a function of experimental parameters such as temperature, stress and probably environment. For the same temperature and environmental conditions, once the stress dependence of the debonding rate is established it is possible to predict the tertiary creep rate of the composite for a different value of applied stress.

2.2 Elastic modulus during tertiary creep

The longitudinal elastic modulus of the 2D woven composite under study has been found to decrease as the damage in the composite increases.[1] The microcomposite model already described can be used to determine a relation between the elastic modulus and the fraction of debonded fibre. The elastic behaviour of block i of the microcomposite is given by:

$$\varepsilon_i^{\mathrm{e}} = \frac{d_i \cdot \varepsilon^{\mathrm{d}} + (\lambda_i - d_i) \cdot \varepsilon^{\mathrm{b}}}{\lambda_i} \tag{9}$$

where ε^{b} and ε^{d} are the elastic strains associated with its bonded and debonded region, respectively. When substituting these elastic strains it should be taken into account that the cross-section in the unbonded region is that of the microcomposite multiplied by a factor $0{\cdot}5V_f$, the fibre volume fraction in the axial direction. Equation (9) may then be rewritten as

$$\frac{1}{E_i} = X_i \frac{1}{0{\cdot}5E_fV_f} + (1 - X_i) \frac{1}{E_b} \tag{10}$$

where E_i, E_f and E_b are the longitudinal elastic modulus of the block i, and of its debonded and bonded regions, respectively. The elastic modulus of the debonded part is in fact that of the fibre, while E_b is given by a simple rule of mixtures. Solving for E_i, eqn (10) becomes:

$$E_i = \frac{E_fV_fE_b}{E_fV_f + (2E_b - E_fV_f)X_i} \tag{11}$$

By adding the elastic elongations corresponding to all the blocks, as given by eqn (9), a similar equation can be established for the elastic modulus of the microcomposite. It reads

$$E(t) = \frac{E_fV_fE_b}{E_fV_f + (2E_b - E_fV_f)X(t)} \tag{12}$$

where $X(t)$ is as defined in eqn (7b).

This expression can also be used to determine the initial fraction of debonded fibre. Calling E_0 the elastic modulus of the damaged composite after loading and completion of the stress redistribution leading to primary creep, and assuming for simplicity that $X_i(0)$ is the same for every block in the microcomposite, this initial fraction is found from eqn (12) as:

$$X_i(0) = X_0 = \frac{\left(\frac{E_b}{E_0} - 1 \right)}{\left(\frac{2E_b}{E_fV_f} - 1 \right)} \tag{13}$$

In this way, the knowledge of the initial debonding conditions and of the evolution equation of the debonding process provides the time evolution of the elastic response for the microcomposite during creep. In first approximation, the elastic behaviour of the 2D woven composite is assumed to be in agreement with that of the microcomposite. Then, eqn (12) is supposed to describe the changes in the longitudinal elastic modulus of the composite.

2.3 Time to first fibre failure

The rupture of the alumina fibre by tensile loading is induced by the growth of flaws present in the intergranular phase. The time to fibre failure is thus a function of the growth rate of these microcracks. Since a progressive debonding takes place during tertiary creep, the part of the alumina fibre

which is continuously exposed to the highest stress during the tertiary stage until the first fibre failure is given by the initial fraction of debonded fibre, as expressed by eqn (13). The largest creep strain will correspond to this part of the fibre, and consequently rupture is expected to occur most likely there. However, since the initial fraction of debonded fibre is stress dependent, the time to first fibre failure will be affected by the variation of both stress and fraction of debonded fibre. A Monkman–Grant approach, which correlates the time to rupture of a fibre to its strain rate during stationary creep, can not be used in such a case because the effect of the fibre length is not considered. A better way to determine the stress dependence of the time to fibre failure during creep of the composite is based on Weibull statistics.[8] Considering a static loading, the cumulative probability of rupture at time t of a fibre of length L under a stress σ may be expressed as:

$$P_w^r(\sigma, t, L) = 1 - \exp\left(-\left(\frac{\sigma}{\sigma'}\right)^m \left(\frac{t}{t'}\right)^b \left(\frac{L}{L'}\right)\right) \quad (14)$$

where σ', t' and L' are constants, m is the Weibull modulus and b is a parameter similarly determined from a Weibull analysis of time to failure. From eqn (14) it follows that for any given failure probability, the rupture times scale as:

$$\left(\frac{t_2}{t_1}\right)^{b/m} = \left(\frac{L_1}{L_2}\right)^{1/m} \frac{\sigma_1}{\sigma_2} \quad (15)$$

In the situation considered here, the ratio of length of fibres has to be replaced by the ratio of the initial fractions of debonded fibre, giving:

$$t_2 = t_1 \left(\frac{X_{01}}{X_{02}}\right)^{1/b} \left(\frac{\sigma_1}{\sigma_2}\right)^{m/b} \quad (16)$$

The Weibull modulus of Sumitomo fibres is close to $m = 7$ at 1100°C.[7] The determination of the parameter b will be discussed in a later section.

2.4 Stress redistribution after fibre failure

The scaling relation in eqn (16) involves the time to the first fibre rupture, which is not necessarily equivalent to the time to composite failure. In fact, the first fibre rupture induces a stress redistribution among the remaining fibres, which may lead to (i) an equilibrium state with a load increase on the remaining fibres, or (ii) a catastrophic failure of the fibre tows and consequently of the composite. The threshold applied stress separating the two behaviours can be determined using the statistical theory of the strength of bundles of threads.[9]

At the end of the debonding process, the composite behaves essentially as an ensemble of a large number of equivalent bare fibres. Therefore, after a fibre failure the load is assumed to be equally redistributed among all the remaining fibres. The applied stress σ after the rupture of some fibres is given by:

$$\sigma = \sigma_0 \cdot \frac{n_0}{n} \quad (17)$$

where σ_0 is the stress before the first fibre failure and n_0 and n are the number of initial and surviving fibres, respectively. Alternatively, the fraction $F(\sigma)$ of fibres which have broken at stress σ is:

$$F(\sigma) = 1 - \frac{n}{n_0} = 1 - \frac{\sigma_0}{\sigma} \quad (18)$$

On the other hand, from eqn (14), the probability of fibre rupture under a stress σ given by Weibull statistics can be expressed as:

$$P_w^r(\sigma) = 1 - \exp(-\alpha \cdot \sigma^m) \quad (19)$$

where $\alpha = 0{\cdot}716$ is calculated from the statistical analysis of the Sumitomo fibre rupture at a high temperature (1000°C).[7]

An equilibrium state featuring a number of surviving fibres and thus avoiding catastrophic rupture can only be obtained if the fraction of fibres which should be broken under a stress σ, as given by eqn (19), is smaller or equal to $F(\sigma)$.[9] Consequently, the threshold stress is the highest value of σ_0 which leads to a possible equilibrium state. The solution to this problem can be obtained graphically. In Fig. 3 both the rupture probability and the fraction of broken fibres are plotted versus the inverse of stress. For a low initial applied stress given by point Q, all possible equilibrium states after load redistribution belong to the region between the two intersection points A and B of the straight line $F(\sigma)$ with the curve $P_w^r(\sigma)$. The transition between catastrophic and non-catastrophic failure is given by point C where

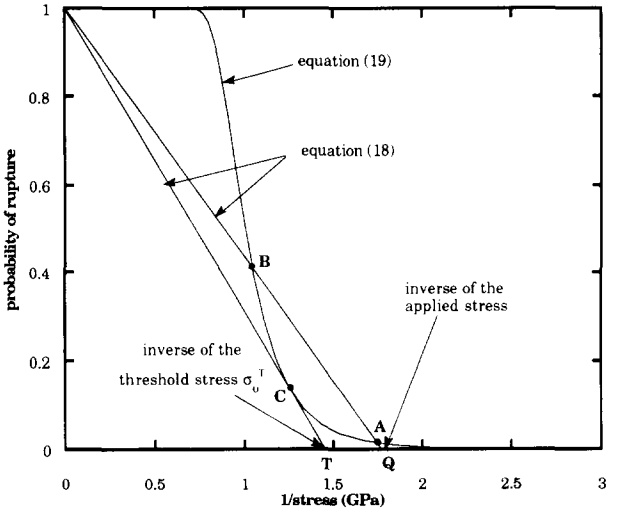

Fig. 3. Graphic analysis of the load redistribution in a bundle of alumina Sumitomo fibres after first fibre rupture.

the straight line is tangent to the curve. The threshold applied stress corresponds to point T. For higher initial stresses than this σ_0^T, $F(\sigma)$ becomes steeper, and there is no value of σ for which an equilibrium state can be attained. With this approach, it is possible to determine the threshold applied stress leading to catastrophic failure after the first fibre rupture occurs for the Al_2O_3(f)/SiC composite.

3 Modelling Results and Discussion

3.1 Creep behaviour at 100 MPa

The distribution of matrix microcrack spacings observed after a creep test at 100 MPa and 1100°C, which is shown in Fig. 6 of Ref. 1, gives an average crack spacing $\bar{p} \cong 1600$ μm. An initial fraction of debonded fibre of $X_0 = 0{\cdot}3$ is found from eqn (13), using the mechanical properties of the composite constituents from Table 1 in Ref. 1 and the initial value ($E_0 = 65$ GPa) of the elastic modulus, found experimentally after the primary creep stage under the same test conditions. Subsequently, a fit of eqn (8) to the experimental strain rate obtained for the early tertiary stage (i.e. when $t < \min(t_i)$) provides a value for the debonding rate $\beta = 21{\cdot}8$ μm/h (see Fig. 4). Once these parameters are known, eqns (2) and (11) give the time evolution of half the length of debonded fibre and of the elastic modulus for a typical elementary block having a length of $\bar{p}$. These curves are shown in Fig. 5. A similar calculation can be performed for the microcomposite, by taking into account the experimentally obtained crack spacing distribution. The result of modelling tertiary creep with eqn (6) is presented on Fig. 6(a) together with the experimental data. In fact, the agreement only comes

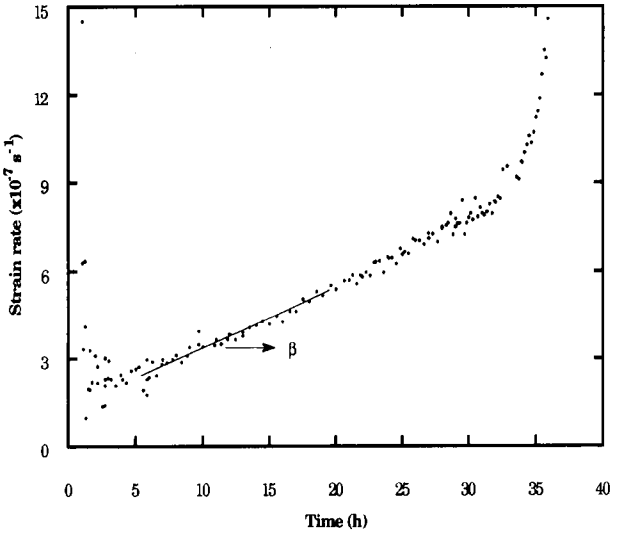

Fig. 4. Evolution of the strain rate during a creep test performed on a 2D Al_2O_3/SiC composite at 1100°C under 100 MPa.

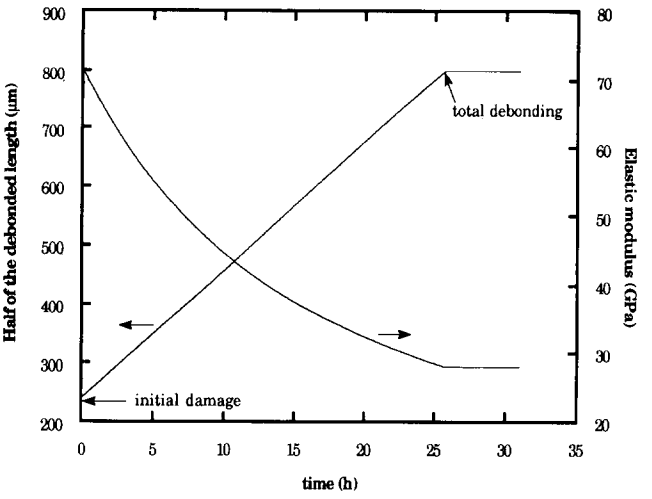

Fig. 5. Modelling of the evolution of the debonded length and the associated change in elastic modulus during creep at 1100°C under 100 MPa for an average microcomposite block.

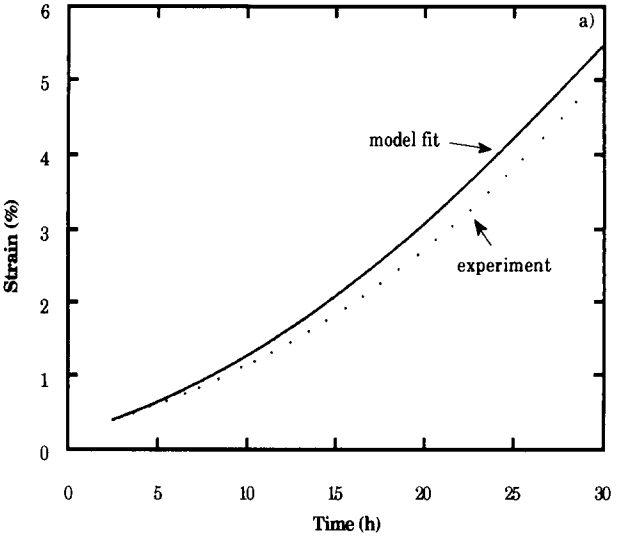

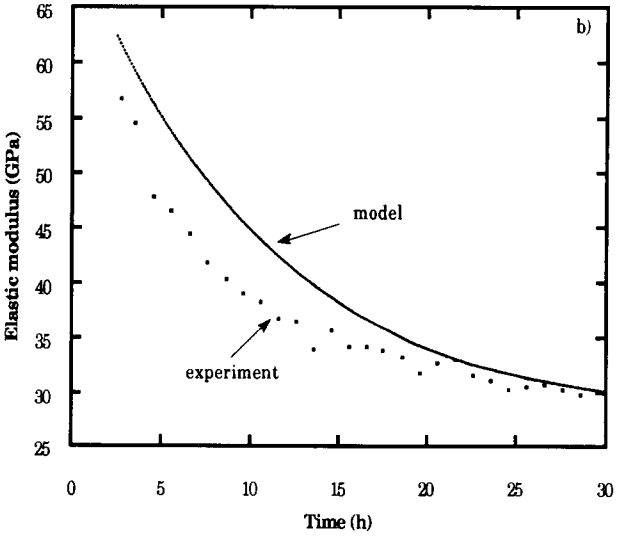

Fig. 6. Evolution of (a) the creep strain and (b) the longitudinal elastic modulus during tertiary creep compared with the modelling results obtained using the microcomposite model.

from the fit to determine the debonding rate β under these experimental conditions. Also, Fig. 6(b) shows the decrease of the composite elastic modulus as function of time during the tertiary creep, as calculated from eqn (12). The agreement of these model curves with experiment shows that a constant debonding rate associated to a crack spacing distribution can model: (i) the tertiary stage of the creep curve and (ii) the change in the elastic response of the composite during creep.

3.2 Predictions at other stresses

After calibration at 1100°C and 100 MPa, the model can be used to predict the tertiary creep behaviour at a different stress. Assuming that for a given temperature the debonding rate is proportional to the fibre creep rate to a first approximation, since debonding results from the evolution of the fibre radial strain, and as the fibre creep rate follows Norton's law,[7] the stress dependence of the debonding rate will also take the form:

$$\beta = \beta^* \left(\frac{\sigma}{\sigma^*}\right)^n \tag{20}$$

where n is the fibre creep stress exponent (here, $n \cong 3$ from Table 1 in Ref. 1). Based on a study of the room-temperature tensile behaviour of the composite,[1] the crack spacing distribution can be assumed not to change in the stress range 100–190 MPa. In fact, when the stress exceeds the elastic limit, matrix crack multiplication is observed to be very limited as compared to the progression of interfacial debonding. The time exponent b appearing in eqn (14) has been evaluated from two creep tests, as follows. At 170 MPa the time to first fibre rupture is given by that of composite failure (2·1 h of tertiary creep after 0·2 h of primary creep, as seen in Fig. 7 of Ref. 1), because a catastrophic rupture occurs. At 100 MPa fibre rupture induces instead a stress redistribution and an increase in the creep rate. In this case, the time to first fibre rupture is taken as the time corresponding to a sudden increase in the curve of the strain rate versus time (29 h of tertiary creep after a primary stage of 2·5 h, as read from Fig. 4). Using these values in eqn (16) gives $b = 1{\cdot}65$.

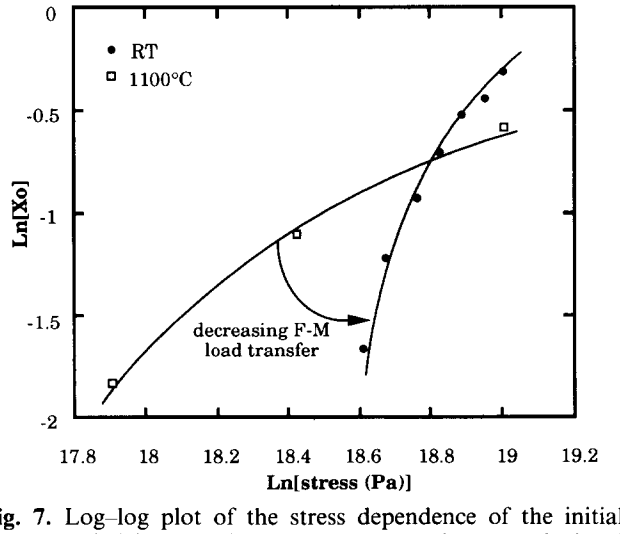

Fig. 7. Log–log plot of the stress dependence of the initial fraction of debonded fibre in the composite, as calculated with eqn (13). The elastic moduli used are obtained from the expermental values in the Figs 2 and 3. The effect of the temperature on the fibre–matrix (F–M) load transfer condition is indicated.

The material parameters in eqn (6) necessary for modelling the creep curve of the composite can be determined as follows. The initial value of the creep strain for tertiary creep, $\varepsilon(0)$ which is the one at the end of the primary stage, has been determined from experiment. The fibre creep rate $\dot{\varepsilon}_f$ under 500 MPa, which corresponds to a composite stress of 100 MPa for a fibre longitudinal volume fraction of 0·2, is given in Table 1 of Ref. 1. The stress dependence of X_0 is found using eqn (13) and it is shown in Fig. 7. The value of the elastic modulus after loading and stress redistribution, E_0, is determined using Fig. 3 of Ref. 1. The stress corresponding to a threshold to catastrophic failure is determined graphically in Fig. 3 from the tangency condition between the two curves. In the case of Sumitomo fibres, this ultimate stress is found to be $\sigma_0^T = 0{\cdot}7$ GPa, which corresponds to a stress of $\sigma_0^T V_f/2 = 140$ MPa applied on the composite. This means that for an applied stress smaller than 140 MPa, load redistribution occurs after the first fibre rupture, whereas catastrophic rupture is expected above that stress. When an equilibrium state can be reached after load redistribution, the surviving fibres experience an increase in their creep rate. The survival time of these remaining fibres is not actually evaluated in this work. Consequently, the calculated tertiary creep curves are not drawn here for times after first fibre failure.

Experimental curves during creep at 1100°C and for stresses of 100, 120, 170 and 190 MPa have been drawn in Fig. 8 together with the corresponding predictions (from eqn (6)) of the present microcomposite model. Also, the stress dependence of the time to rupture (from eqn (16)) is presented in Fig. 9. From these results, several comments arise:

(1) The initial creep rates obtained with the model agree with experiment (Fig. 8). The general aspect of the tertiary creep curves is clearly provided by the model: the change of the creep rate with time is more pronounced at low stress than at high stress. This phenomenon results from the fact that there is a higher potential of damage at low creep stress than at high creep stress.

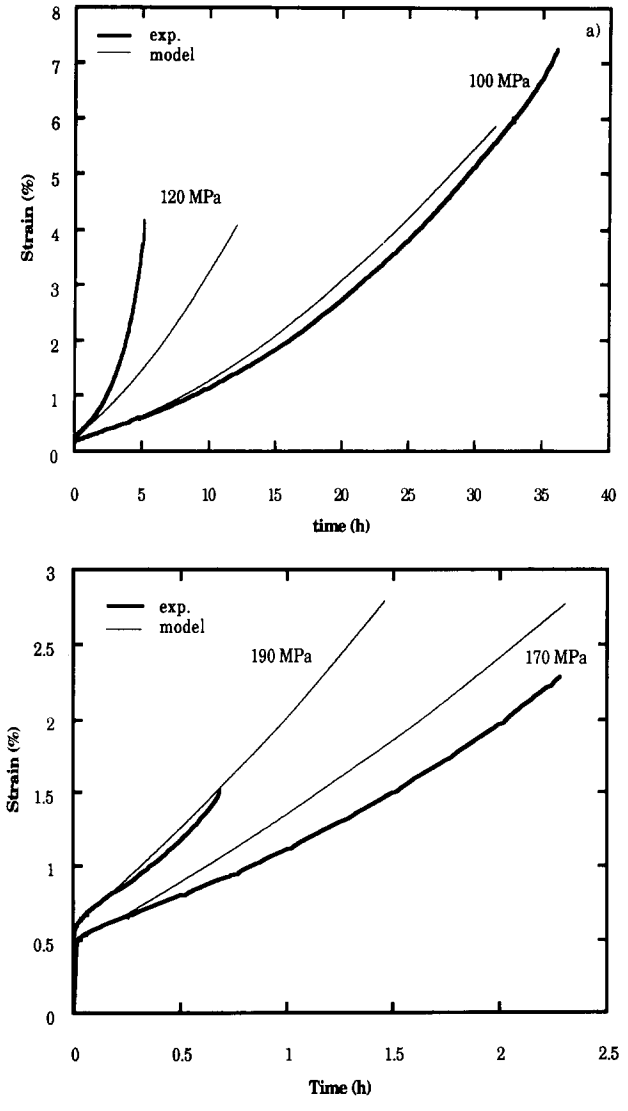

Fig. 8. Predictions of the microcomposite model compared to the corresponding experimental[1,3] creep curves at 1100°C under (a) 100 MPa; 120 MPa and (b) 170 MPa; 190 MPa.

(2) From Fig. 8, it seems that eqn (16) overestimates the time to rupture of the composite, especially for the highest creep stress. However, Fig. 9 shows that the global stress dependence of the time to composite rupture is reproduced well using Weibull statistics.

(3) A decrease of the strain to rupture when the level of stress increases is observed in Fig. 8. This phenomenon, which is described by the model, results from a competition between the debonding process and the creep of the fibre during the tertiary stage.

(4) The rupture mode of the composite depends on the level of the stress. A threshold applied stress can be calculated in order to determine the transition between catastrophic and non-catastrophic failure.

(5) The main success of this model is to be in good agreement with the experimental stress dependence of the minimum creep rate. Previous work[4] has observed that the stress exponent of the minimum creep rate decreases when the creep stress increases from 100 MPa to 190 MPa. The creep rate calculated from the model also reflects such a behaviour. The evolution in the stress exponent can be related to the stress dependence of the damage state of the composite right before the initiation of the tertiary stage. In fact, as expressed by eqn (8), this initial tertiary creep rate is the product of the fibre creep rate times the initial fraction of debonding which increases with the level of stress. At high stresses, X_0 is close to one, and the composite behaves like a bundle of alumina fibres. The stress exponent is then in practice that of the fibre. With lower creep stress, X_0 decreases (Fig. 7) and the calculated creep rate of the composite becomes smaller than that of alumina fibres, thus resulting in an apparent increase of the creep stress exponent. As a consequence, an effective stress exponent cannot be determined for the creep behaviour of this damageable composite, because the creep rate depends on the initial state of damage.

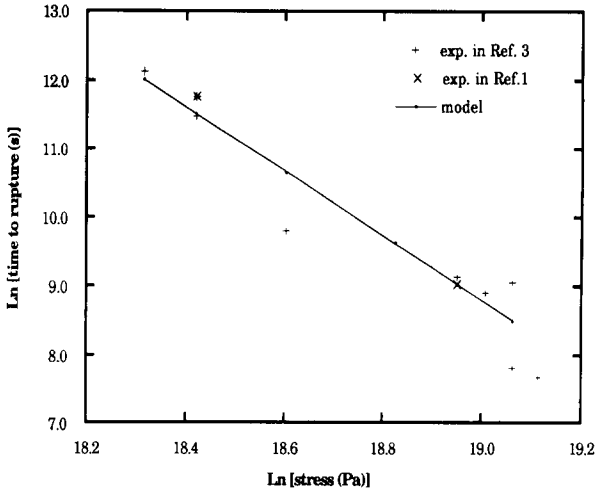

Fig. 9. Stress dependence of the time to composite rupture at 1100°C.

The stress dependence of the creep rate for the alumina fibre and silicon carbide matrix material is represented in Fig. 10 by straight lines.[1] In this figure, the values on the stress axis correspond to the stress applied on the composite. The stress on the fibre and on the matrix is found by dividing the composite stress by their respective volume fractions $V_f/2 = 0{\cdot}2$ for the longitudinal direction and $V_m = 0{\cdot}4$. The values of the creep rate of the Al_2O_3(f)/SiC composite calculated with the model have also been plotted in Fig. 10, which illustrates well the dependence of the creep stress exponent on the initial state of damage of the composite.

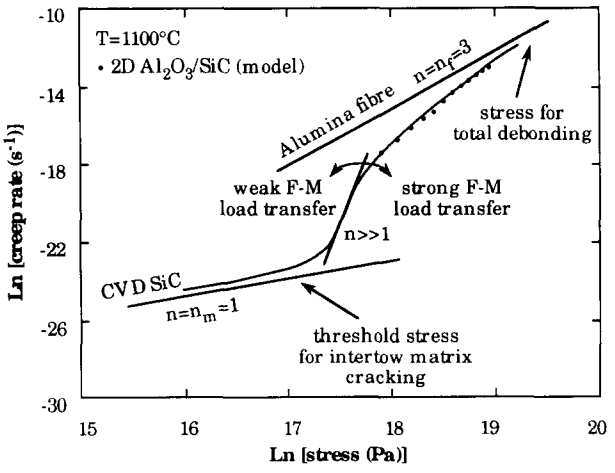

Fig. 10. Plot of the minimum creep rate versus stress for the CVD SiC matrix, the alumina Sumitomo fibre, and the modelled 2D Al_2O_3/SiC composite. Included is the effect of the fibre–matrix (F–M) load transfer condition on the apparent stress exponent.

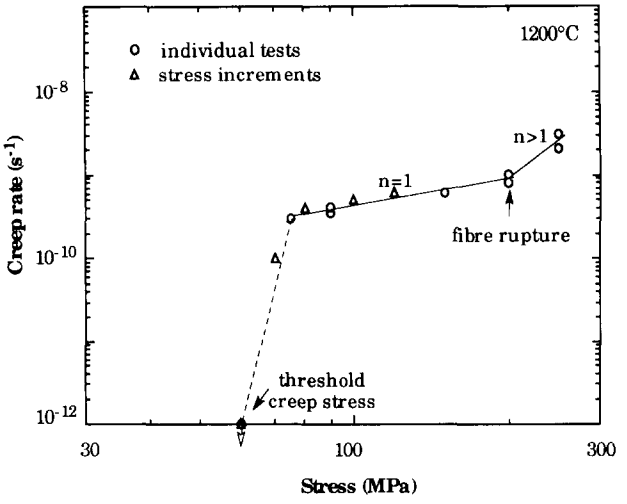

Fig. 11. Creep rate versus applied tensile stress for a SiC-fibre (SCS-6) Si_3N_4 matrix (HPSN) composite.

Namely, for high stresses the creep behaviour is controlled by fibre creep, while for stresses smaller than the matrix cracking stress, the stress exponent corresponds to that of the matrix, the more creep resistant constituent.

Between these two limiting cases, the creep rate monotonically increases with applied stress. The first deviation from linearity in the log–log plot, reflecting an increase of the apparent stress exponent, corresponds to the matrix cracking stress (for the uncracked matrix located between the fibre tows, see Ref. 1). The second qualitative change, corresponding to the decrease of the apparent stress exponent which is found experimentally, is related to the onset of fibre-controlled creep. The transition between these two stages induces necessarily high apparent stress exponents. The same analysis of the change in the creep stress exponent can be applied to the 1200°C tensile creep of 0° SiC (SCS-6)/Si_3N_4(HPSN) composites, described in Ref. 10. In Fig. 11, it can be observed that above the region with a dashed line the stress exponent (n = 1) is given by that of the more creep resistant constituent, here the SCS-6 SiC fibre. Above the stress associated with fibre rupture (200MPa), an increase of the stress exponent is observed (n > 1). This change in the stress exponent is similar to the one observed in the Al_2O_3(f)/SiC composite at low stress.

For this latter composite, the shape of the transition between the two non-linear stages of the curve in Fig. 10 depends on the rate of damage accumulation. In the case of low fibre–matrix load transfer (weak interphase), a short transition is expected, associated to high apparent stress exponents. In contrast, a strong interphase is expected to lead to a more extended transition with low apparent stress exponents. A possible way to observe the effect of the fibre–matrix load transfer conditions on the apparent stress exponents is to perform creep tests at lower temperatures. At lower temperatures, the mismatch of thermal expansion coefficient between fibre and matrix in the radial direction induces a weaker interphase, because of the radial shrinkage of the fibre with respect to the matrix. The decrease of the load transfer capability implies that the debonding process becomes strongly stress dependent as it is observed in Fig. 7. Therefore, an increase of the apparent stress exponent for creep when temperature decreases is expected to confirm the influence of fibre–matrix load transfer conditions on the creep behaviour.

4 Conclusions

The tertiary creep of an Al_2O_3(f)/SiC composite has been modelled on the basis of progressive fibre–matrix debonding and of fibre failure mechanisms:

(1) The modelling results explain the behaviour of the tertiary creep strain and the corresponding evolution of the longitudinal elastic modulus of the composite.
(2) The times to rupture are well described by an approach based on Weibull statistics, which takes into account the effect of stress and the fraction of fibre loaded.
(3) The difference in the composite failure mode at low and high creep stresses has been attributed to the possibility or not for the composite to reach an equilibrium state after the first fibre rupture.
(4) The stress dependence of the apparent stress exponents has been correlated with the damage state of the composite at the

secondary stage. An interpretation of the changes in the apparent stress exponent has been suggested, based on a possible transition from creep controlled by the most creep resistant component to creep controlled by the least resistant one.

Acknowledgements

This work has been performed within the Specific Research and Development Programme of the European Commission. The authors thank M. Bourgeon and J. M. Parenteau (SEP) for providing the material.

References

1. Lamouroux, F., Steen, M. & Vallés, J. L., Uniaxial tensile and creep behaviour of an alumina fibre-reinforced ceramic matrix composite: I. Experimental study. *J. Eur. Ceram. Soc.*, **14** (1994) 529–37.
2. Holmes, J. W. & Chermant, J. L., Creep behaviour of fibre-reinforced ceramic matrix composites. In *High Temperature Ceramic Matrix Composite, Proceedings of the 6th European Conference on Composite Materials*, ed. R. Naslain, J. Lamon & D. Doumeingts. Bordeaux, 1993, pp. 633–47.
3. Adami, J. N., Comportement en fluage uniaxial sous vide d'un composite 2D Al_2O_3/SiCl, Thesis, Ecole Polytechnique de Zurich, Switzerland, 1992.
4. Adami, J. N., Bressers, J. & Steen, M., *Proceedings of the Conference of Materials*, Lisbon, 1991, pp. 571–83.
5. Steen, M. & Vallés, J. L., Uniaxial creep of ceramic matrix composites: experiments and modelling. In *Mechanisms and Mechanics of Composite Fracture*, ed. R. B. Bhagat, S. G. Fishman & R. J. Arsenault. ASM, Pittsburgh, 1993.
6. Kotil, T., Holmes, J. W. & Comninou, M., Origin of hysteresis observed during fatigue of ceramic–matrix composites. *J. Am. Ceram. Soc.*, **73** (1990) 1879–83.
7. Lesniewski, Ch., Aubin, C. & Bunsell, A. R., Property–structure characterization of a continuous fine alumina–silica fibre. *Composites Science and Technology*, **37** (1990) 63–78.
8. Snowden, W. E., Surface flaws and the mechanical behavior of glass optical fibers. In *Fracture Mechanics of Ceramics; Vol. 3: Flaws and Testing*, ed. R. C. Bradt, D. P. H. Hasselman & F. F. Lange. Plenum Press, NY, 1978.
9. Daniels, H. E., The statistical theory of the strength of bundles of threads. I. *Proc. R. Soc. London*, **A183** (1945) 405–35.
10. Holmes, J. W., Park, Y. H. & Jones, J. W., Tensile creep and creep–recovery behavior of a SiC-fibre–Si_3N_4-matrix composite. *J. Am. Ceram. Soc.*, **75** (1993) 1281–93.